Tellus
SERIES B
CHEMICAL
AND PHYSICAL
METEOROLOGY
PUBLISHED BY THE INTERNATIONAL METEOROLOGICAL INSTITUTE IN STOCKHOLM

Tellus (2009), 61B, 394–407
Printed in Singapore. All rights reserved

TELLUS

Exploring CO pollution episodes observed at Rishiri Island by chemical weather simulations and AIRS satellite measurements: long-range transport of burning plumes and implications for emissions inventories

By HIROSHI TANIMOTO[1,2,3]*, KEIICHI SATO[1], TIM BUTLER[4], MARK G. LAWRENCE[4], JENNY A. FISHER[5], MONIKA KOPACZ[3], ROBERT M. YANTOSCA[3], YUGO KANAYA[6], SHUNGO KATO[7], TOMOAKI OKUDA[8], SHIGERU TANAKA[8] and JIYE ZENG[2,1]*Asian Environment Research Group, National Institute for Environmental Studies, Tsukuba, Japan;* [2]*Center for Global Environmental Research, National Institute for Environmental Studies, Tsukuba, Japan;* [3]*School of Engineering and Applied Sciences, Harvard University, Cambridge, USA;* [4]*Atmospheric Chemistry Department, Max Planck Institute for Chemistry, Mainz, Germany;* [5]*Department of Earth and Planetary Sciences, Harvard University, Cambridge, USA;* [6]*Frontier Research Center for Global Change, Japan Agency for Marine-Earth Science and Technology, Yokohama, Japan;* [7]*Faculty of Urban Environmental Sciences, Tokyo Metropolitan University, Tokyo, Japan;* [8]*Faculty of Science and Technology, Keio University, Yokohama, Japan*

(Manuscript received 16 May 2008; in final form 24 October 2008)

ABSTRACT

The summer of 2003 was an active forest fire season in Siberia. Several events of elevated carbon monoxide (CO) were observed at Rishiri Island in northern Japan during an intensive field campaign in September 2003. A simulation with a global chemistry-transport model is able to reproduce the general features of the baseline levels and variability in the observed CO, and a source attribution for CO in the model suggests that the contribution from North Asia dominated, accounting for approximately 50% on average, with contributions of 7% from North America and 8% from Europe and 30% from oxidation of hydrocarbons. With consideration of recent emission estimates for East Asian fossil fuel and Siberian biomass burning sources, the model captures the timing and magnitude of the CO enhancements in two pollution episodes well (17 and 24 September). However, it significantly underestimates the amplitude during another episode (11–13 September), requiring additional CO emissions for this event. Daily satellite images from AIRS reveal CO plumes transported from western Siberia toward northern Japan. These results suggest that CO emissions from biomass burning in western Siberia in 2003 are likely underestimated in the inventory and further highlight large uncertainties in estimating trace gas emissions from boreal fires.

1. Introduction

Carbon monoxide (CO) is often measured in a subsidiary manner with other trace species such as tropospheric ozone (O_3) and black carbon (BC). Tropospheric O_3 has a variety of important roles in the earth's environment, including detrimental effects on vegetation and human health and global warming as a greenhouse gas. Tropospheric O_3 is photochemically generated, and the detailed understanding of chemistry involved in O_3 formation and destruction is still imperfect. BC is emitted from combustion sources, contributing to the heating of the atmosphere by absorbing solar radiation and to severe air pollution near the ground surface. CO is commonly utilized as a relatively long-lived tracer of combustion to characterize contributions from various types of surface sources and/or diagnose subsequent chemical processing of secondary species. For example, the relationships of O_3 versus CO provide information on net production or destruction of O_3 per emitted CO (as a

*Corresponding author.
e-mail: tanimoto@nies.go.jp
DOI: 10.1111/j.1600-0889.2008.00407.x

proxy for O_3 precursors), leading to better characterization of regional photochemistry (e.g. Parrish et al., 1993, 1998). Both BC and CO are primarily emitted from inefficient combustion processes, and the relative abundance depends on the composition and type of the fuel, the amount of available oxygen and the degree of oxidation. Hence relationships of BC versus CO downwind of, but close to source regions provide an opportunity to estimate emission ratios of BC with respect to CO from combustion sources (e.g. fossil fuel, biomass burning or biofuel), leading to improvement in emissions inventories (e.g. Dickerson et al., 2002).

Spatial distributions and temporal variations of CO itself are also useful for evaluating the emission strength of CO from various sources and regions. Since the reduction of CO emissions from human-related activities can be achieved by rapid shifts in energy types (e.g. from biofuel to oil or electricity), accurate estimates are difficult for regions experiencing rapid economic growth (Streets et al., 2006; Tanimoto et al., 2008a). Biomass burning is also a major source for CO. CO emissions from biomass burning have substantial interannual variability, often prohibiting accurate emission estimates. Hence, analysis of variations and distributions of CO in individual field measurements, especially with chemistry-transport models, can help understand regional CO sources in detail and improve existing emissions inventory for CO.

In this paper, we report on continuous measurements of CO and O_3, along with intensive measurements of other gaseous and aerosol components performed at the northernmost remote Japanese island of Rishiri in September 2003. We identify several pollution episodes using multiple gaseous and aerosol tracers. By analysing in situ measurements together with chemical weather simulations, we quantitatively discuss the contributions from each source to the day-to-day variations of CO and highlight one of the observed high CO episodes. Daily satellite images for CO total columns reveal possible source regions and transport paths to Rishiri Island and suggest the importance of CO sources that are not accounted for in current emissions inventories for biomass burning in Siberia.

2. Field measurements and analytical tools

2.1. Observation site

Measurements described here were made on Rishiri Island, a remote small island located between the northernmost large Japanese island (i.e. Hokkaido) and the Eurasian continent. The Rishiri Island observatory (RIS, 45.07°N, 141.12°E, 35 m a.s.l.) is located in the southwest of the island. Local pollution from the industrial activities on the island is negligible. Previous studies based on backward trajectory analyses showed that air masses arriving at the site are influenced by air masses from the continent throughout the year. Rishiri Island occasionally experiences pristine maritime air masses during summer, but the influence of maritime air masses from the Pacific Ocean is very weak compared with southern Japan. The continental air masses frequently come from Siberia, and anthropogenically polluted air masses occasionally arrive, being influenced by emissions from China, Korea and Japan (Tanimoto et al., 2002). Hence, the main sources of pollution for this region are human-induced emissions in East Asia and biomass burning in Siberia.

2.2. Measurements of tracers

We started continuous measurements of O_3 and CO at Rishiri in 1998 as a part of a long-term monitoring program. The measurements at Rishiri have been characterized by previous studies (e.g. Tanimoto et al., 2000, 2002). One of notable characteristics at Rishiri is that Siberian wildfires often influence chemical composition and surface air quality, as observed in summer of 1998 (Tanimoto et al., 2000; Yurganov et al., 2004) and 2002 (Yurganov et al., 2005) and spring of 2003 (Jaffe et al., 2004; Tanimoto et al., 2008b).

In addition to routine monitoring of O_3 and CO, a variety of chemical components, including reactive species and long-lived tracers along with radiatively important parameters, were measured as part of an intensive field campaign in September 2003. The observations include BC, non-methane hydrocarbons (NMHCs), organo-halogens and aerosol particle number densities, as described in detail in Kanaya et al. (2007).

Briefly, the mixing ratios of O_3 and CO were determined using photometric instruments based on absorption in the ultraviolet and infrared wavelength regions, respectively. The O_3 instrument utilized absorption at 253.7 nm emitted by a low-pressure mercury lump (Dylec, model 1150) and was calibrated by a working standard maintained by our laboratory. The CO instrument was based on non-dispersive absorption (Kimoto, model 541) and was calibrated by a gravimetric gas standard at 1.8 ppmv (Tanimoto et al., 2000). Light attenuation by BC was determined by an aethalometer (Magee Scientific, model AE-16) at a single wavelength of 880 nm. Aethalometer-derived BC concentrations can significantly be affected by the uncertainty associated with the mass absorption efficiency of BC. Here we followed the manufacturer's recommendation and used an instrumental factor of 16.6 $m^2\ g^{-1}$ at a wavelength of 880 nm. Particles were sampled without a size cut-off separator, and hence concentrations in all size ranges were measured for BC, which is typically in the sub-micron mode. The Magee aethalometer instrument was compared with another optical instrument (Kimoto, model OBC) prior to the campaign, and a good correlation between two instruments was found. The Kimoto OBC instrument determines BC concentrations based on reflectance of light. We have often used the Kimoto instrument as our 'reference' BC measurement, since it was compared with other thermal and thermal/optical methods to determine concentrations of carbonaceous aerosols, and the degree of agreement with thermal/optical methods provided by DRI carbon analyser

(DRI, model 2001) has been characterized in a separate study (Hasegawa et al., personal communication, 2007). Number densities of aerosol particles were measured as a function of size using a combination of a scanning mobility particle sizer (TSI, model 3936) and an optical particle counter (Rion, KC18) with size bins of >0.1, >0.15, >0.2, >0.3 and >0.5 μm (Kanaya et al., 2007). The chemical composition of the aerosol was analysed by filter sampling followed by ion chromatography. The sampling was made at 24-h intervals using a low-volume sampler (Okuda et al., 2006). Daily whole-air sampling was made using Silco-steel 3-L canisters (Restek). The air samples were then analysed following the campaign using GC-FID and GC-MS systems coupled with a pre-concentration system (Kato et al., 2004). More than 36 volatile organic compounds were determined, including acetylene and C_2Cl_4, as will be shown later.

2.3. Chemical weather simulation

For data analysis, output from an operationally available chemical weather forecast and analysis system was used. The chemical weather forecast and analysis system used is based on the global three-dimensional chemistry transport model 'Model of Atmospheric Transport and Chemistry'—Max Planck Institute for Chemistry version (MATCH-MPIC; Rasch et al., 1997; Lawrence et al., 1999; Lawrence et al., 2003; von Kuhlmann et al., 2003), and the output of which is available online at http://www.mpch-mainz.mpg.de/∼lawrence/forecasts.html. The MATCH-MPIC simulations were driven by wind, temperature, pressure, surface heat flux and surface-wind stress data from the NCEP/NCAR reanalysis, at T42 horizontal resolution (roughly 2.8° in latitude and longitude), and with 42 vertical levels (from the surface to about 2 hPa). The setup used here is the same as described in detail in Lawrence et al. (2003), with the exception that the CO tracers are additionally broken down into their fossil fuel and biomass burning components. The model includes tropospheric chemistry with representations of basic methane chemistry, plus ethane, propane, ethene, propene, n-butane and isoprene oxidation; surface sources from fossil fuel burning, biomass and biofuel burning, soils and oceans; sources from lightning, aircraft and stratosphere–troposphere exchange; online reaction rates and photolysis rates which are updated each time step and sinks due to wet and dry deposition. Briefly, surface emissions of CO, which we will call 'standard' emissions and discuss later, are based on a combination of the Emission Database for Global Atmospheric Research (EDGAR) inventory version 3.2 (for the year 1995; Olivier and Berdowski, 2001; Olivier et al., 2002) for industrial emissions and Galanter et al. (2000) and Andreae and Merlet (2001) for biomass burning, as detailed in Lawrence et al. (2003) and von Kuhlmann et al. (2003). Biomass burning emissions include waste burning and fuel use as well as fire emissions. We also tested biomass burning emissions from the Global Fire Emissions Database version 2 (GFEDv2; van der Werf et al., 2006) to examine the sensitivity of the results to the emissions inventory, in particular CO emissions from biomass burning in Siberia by using the GFEDv2 time-varying monthly emissions inventory constructed from satellite-detected hotspots. Since GFEDv2 data do not include waste burning and fuel use, these classes were added to the GFEDv2 inventory, and hence this set is called as 'hybrid-GFEDv2' emissions.

3. Results and discussion

3.1. Temporal variations of carbon monoxide in summer—fall 2003

It is well known that Siberia experienced substantial wildfires in 2003. Yurganov et al. (2005) reported widespread enhancement of CO in the summer of 2003 in the Northern Hemisphere, due to wildfires in Siberia. According to the GFEDv2 inventory, the fire activities in 2003 intensively started in May in eastern Siberia (around Lake Baikal), reaching the maximum in May–July period, and moved eastwards to far eastern Siberia (Yakutia and Magadan/Kolyma) in July–August. In September, the fire intensity decreased, but fires were still significant. Figure 1 exhibits summertime mixing ratios of CO and O_3 from July to September 2003, along with normalized mean seasonal cycle of CO derived from 7-yr measurements from 1998 to 2004. The mean CO seasonal cycle is at the minimum in mid-July and starts recovering in early August toward fall, in good

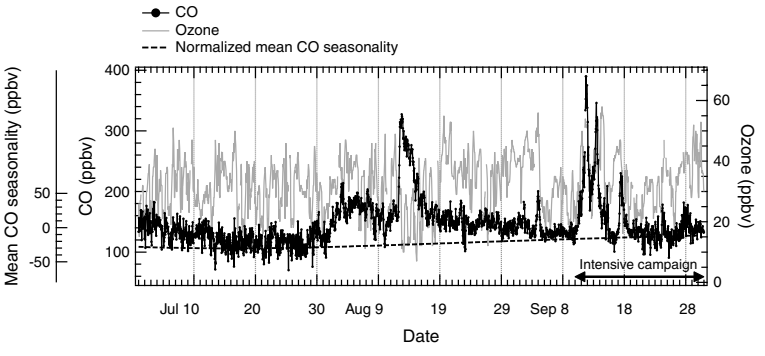

Fig. 1. Time-series of CO and O_3 observed at Rishiri Island from July to September 2003. Also shown is normalized mean CO seasonal cycle.

accordance with general seasonal pattern in this northern mid-latitude zone. The increase from July to September is about 20 ppbv. In 2003 the CO baseline was greatly enhanced in August, and several remarkably high episodes were observed. In particular, the episodes during 12–15 August and 11–13 September showed high CO levels, whose peaks exceeded 300 ppbv. The enhancement of CO around 17 September was also apparent. The CO levels in latter half of September were relatively stable.

Considering fire activities in the summer of 2003, the modulation in the baseline and elevated events of CO at Rishiri in August are likely caused by large-scale impacts of Siberian wildfires. The intensive campaign we describe here covered three weeks until the end of September, and the intensity of Siberian fires started to drop down from August toward fall. However, the burnings were still significant. Hence, measurements at Rishiri during the campaign likely had influences from Siberian wildfires, in addition to anthropogenic influences from East Asia, a common pollution source in this Pacific rim region, regardless of the year. It should be noted that the magnitude of elevated CO during 11–13 September was larger than that observed during 12–15 August. Time-series of O_3 during the summer period had large variability resulting from combination of day-to-day and diurnal variations, and they essentially provide little clue about modification of the CO baseline and high CO-episodes. We focus on the September intensive campaign, when measurements of multiple tracers were performed.

3.2. *Temporal variations of trace gases and aerosols during an intensive campaign*

Temporal variations of CO, BC, O_3, aerosol number density, selected aerosol components and long-lived tracers of industrial activities (C_2Cl_4, C_2H_2) obtained during the intensive field campaign in September 2003 are shown in Fig. 2. Mean mixing ratios

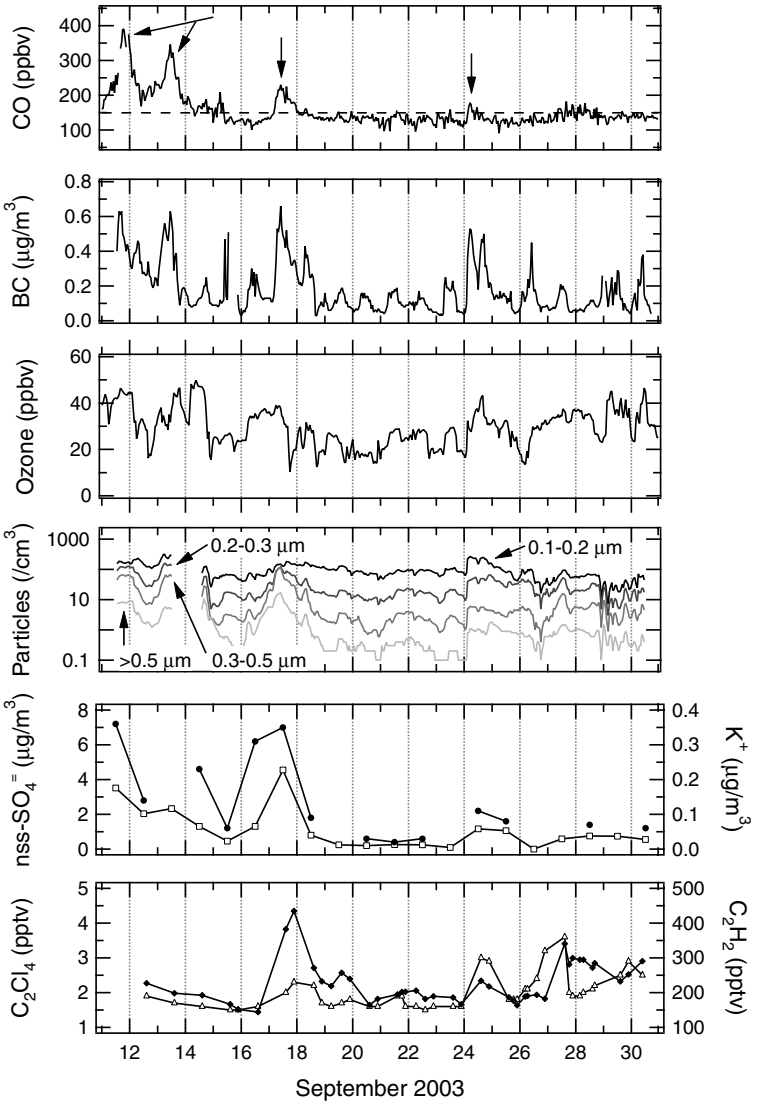

Fig. 2. Temporal variations of CO, BC, O_3, particles, non-sea salt sulphate, potassium, tetrachloroethylene and acetylene, observed at Rishiri Island in September 2003. Arrows indicate high episodes on 11–13, 17 and 24 September 2003. The dashed horizontal line denotes the mean mixing ratio of CO during this period. Time axis is local time (UTC + 9 h).

of CO during the intensive measurement period were 150 ppbv (indicated by a dashed line for CO). Temporal variations of CO, a good indicator for the emissions from combustion processes, showed enhancement during 11–13, 17 and 24 September 2003 (indicated by arrows). The 11–13 September event exhibited two large peaks reaching 389 ppbv (11 September) and 346 ppbv (13 September), an enhancement of 200–250 ppbv above the mean mixing ratios. The maximum mixing ratios observed on 17 and 24 September were 230 and 178 ppbv, respectively, and were not as high as those on 11–13 September.

The enhancements in O_3 were not as remarkable as those in CO due to the generally large variability in O_3. Large variability in O_3 could be caused by micrometeorology that occasionally prevails in the absence of strong westerly winds, daytime photochemistry and nighttime dry deposition. However, there still seem to be enhancements in O_3 corresponding to CO, reaching approximately 45 ppbv in these three events. The amount of BC determined by the aethalometer was enhanced at the same times as CO, peaking at 0.63, 0.66 and 0.53 $\mu g\,m^{-3}$, on 11–13, 17 and 24 September, respectively. The BC concentrations fall in the range of those observed in springtime of 2001 at the same site (Matsumoto et al., 2003a). Although there are some data lacking for particle number density around 14 September, enhancements on 17 and 24 September are clear at the same timing with CO and BC in all size bins. For example, the number density for 0.1–0.2, 0.2–0.3, 0.3–0.5 and 0.5 μm size bins jumped up from 100, 20, 2 and 0.1 per cm^3, respectively, on 23 September to 240, 50, 6 and 1 per cm^3, respectively, on 24 September. Temporal variations of non-sea salt (nss-) sulphate showed large enhancements on 17 September, reaching 4.5 $\mu g\,m^{-3}$, as well as a small increase on 24 September, with a moderate concentration level (2–3 $\mu g\,m^{-3}$) during 11–13 September. These numbers are in good agreement with Matsumoto et al., (2003b), who reported that the maximum nss-sulphate concentrations in springtime of 2001 reached as high as 9.22 $\mu g\,m^{-3}$, with a mean concentration of 2.48 $\mu g\,m^{-3}$. Potassium in the aerosol phase can be used as an indicator for biomass burning (Novakov et al., 2000). Potassium also showed enhancements on 17 and 24 September, peaking at 0.35 and 0.11 $\mu g\,m^{-3}$, respectively. In contrast to these events, during 11–13 September the magnitude of the peak in potassium was larger than that in nss-sulphate, suggesting an additional influence (e.g. biomass burning) on potassium. Tetrachloroethylene (C_2Cl_4) and acetylene (C_2H_2) can be used as good tracers for industrial activities. Large enhancements were seen on 17 and 24 September, particularly for C_2H_2, which peaked at 434 pptv on 17 September. Although data on these species were not available on 11 September, enhancements on 13 September were not observed for either C_2Cl_4 or C_2H_2. The co-elevation of BC and nss-sulphate observed during these events can be attributed to the pollution from Asian continental sources (likely coal combustion), as often observed in the marine boundary layer sites of the western North Pacific (Kaneyasu and Murayama, 2000; Matsumoto et al., 2003b; Kaneyasu and Takada, 2004).

Figure 3 shows scatter plots of O_3 versus CO observed in 2003 September, including the three high episodes. Also plotted is the correlation of O_3 and CO observed during 1998 September, when Rishiri Island was subject to outflow from severe boreal forest fires that occurred in Siberia (Yurganov et al., 2004). A previous report suggested that CO was greatly enhanced, but O_3 was only slightly elevated (Tanimoto et al., 2000). One of possible causes for the small O_3 enhancements is that location of fires was very close to Rishiri Island, and therefore, O_3 formation did not efficiently occur in such fresh air masses. Here, the data in 1998 cover a slightly larger mixing ratio range than in 2003 for both O_3 and CO, suggesting that background levels for these trace gases were also influenced in 1998. The data from the two episodes on 17 and 24 September are in good accordance with the data from the rest of the intensive period. In contrast, the O_3–CO correlation during 11–13 September shows a large enhancement in CO with only a small enhancement in O_3. This is very similar to what was observed in 1998, implying that it is likely that there was an influence from forest fires in Siberia during the 11–13 September episode.

In addition to the O_3–CO relationship, the BC to CO relationship may provide further information to help identify dominant sources influencing the chemical composition in the observed air masses. Scatter plots of BC versus CO observed in September 2003 are also shown in Fig. 3. Both CO and BC are primary compounds emitted from combustion processes, often resulting in reasonably good correlation, although the relative enhancement

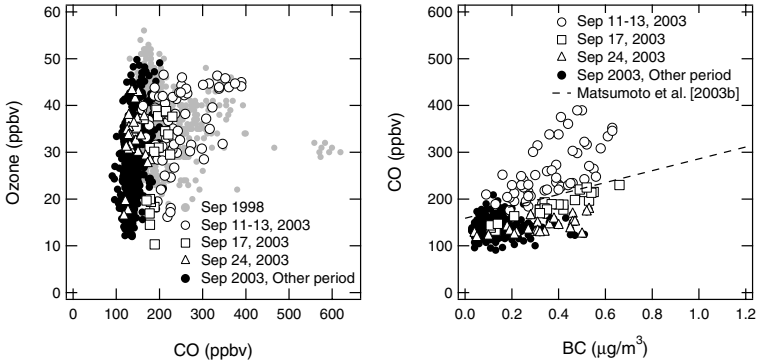

Fig. 3. Left-hand panel: scatter plots of O_3 versus CO during September 2003, overlaid on those during September 1998. Right-hand panel: scatter plots of BC versus CO during September 2003. The three events are given separate symbols. The dashed line is the regression line for CO to BC derived from Matsumoto et al. (2003b) for the spring of 2001.

(i.e. $\Delta BC/\Delta CO$) can differ, depending on the source types. Black carbon was enhanced during all three events on 11–13, 17 and 24 September. However, the relative enhancement during the 11–13 September is different from the 17 and 24 September events. The regressions for the three events provide $\Delta BC/\Delta CO$ ratios of 0.0013 μg m^{-3}ppbv^{-1} (11–13 September), 0.0046 μg m^{-3} ppbv^{-1} (17 September) and 0.0047 μg m^{-3} ppbv^{-1} (24 September). The $\Delta BC/\Delta CO$ ratios determined on 17 and 24 September are similar to those measured at the same site in the air masses transported from polluted regions of the Asian continent in the spring of 2001 (Matsumoto et al., 2003b). This suggests that the air masses observed on 17 and 24 September are influenced by anthropogenic sources (e.g. fossil fuel emissions) from East Asia. The maximum BC concentrations observed in this study (0.6 μg m^{-3}) are in the range from 0.6 μg m^{-3} (Matsumoto et al., 2003b) to >1.5 μg m^{-3} (Kaneyasu and Murayama, 2000), which are the maximum concentrations in the marine boundary layer observed in Asian pollution plumes. By contrast, the $\Delta BC/\Delta CO$ ratios observed during 11–13 September were much lower than those observed by Matsumoto et al. (2003b), suggesting that the air masses had different characteristics in terms of BC and CO. Biomass burning plumes generally have a different BC versus CO emission ratio compared with fossil fuel combustion. Large enhancements in BC relative to CO ware reported in biomass burning plumes in subtropical regions (Dickerson et al., 2002). For boreal fires, smoke plumes from Siberian fires in May 2003 were observed at a high altitude site on the summit of Mt. Fuji. The mean $\Delta BC/\Delta CO$ ratio observed in fire plumes transported in the free troposphere from Siberia was 3.7 $\times$ 10^{-3} g BC per g CO (Kaneyasu et al., 2007), which is twice as large as the relative abundance (1.6 $\times$ 10^{-3} g BC per g CO) observed here in the marine boundary layer in September 2003. We observed lower BC enhancement relative to CO here for the 11–13 September event, disagreeing with Kaneyasu et al. (2007) and being contrary to speculation from the O_3–CO correlations. One of possible reason for the lower $\Delta BC/\Delta CO$ ratios observed at Rishiri Island was that BC was effectively removed during transport in the boundary layer by scavenging or wet deposition.

The resulting speculations from correlative behaviours of O_3 to CO and of BC to CO do not provide for unambiguous conclusions. The problems associated with interpretation in field measurements made downwind of the continental sources but not close to the sources themselves could often stem from significant uncertainties of available information. Aerosol is easily modified during the transport and is deposited with poorly quantified rate, depending on meteorology. Emission ratios of trace gases emitted by biomass burning dramatically depend on burning conditions, regions and biomass types. The injection heights of burning emissions affected by fire intensity and local meteorology provide an additional uncertainty. These uncertainties could result in controversial interpretation for various tracers.

3.3. Analysis with MATCH-MPIC simulations

To further explore the possible sources affecting elevated CO (and other tracers) and discuss their impacts quantitatively, we utilized simulations of a global chemistry-transport model. Figure 4 shows a comparison of observed and MATCH-MPIC modelled mixing ratios of O_3 and CO at Rishiri Island during the

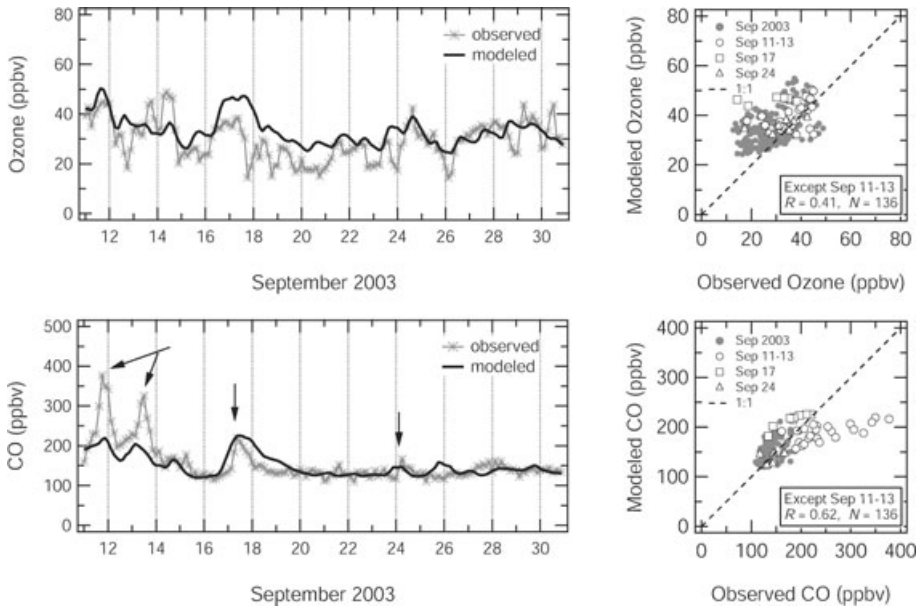

Fig. 4. Model predicted O_3 (upper panel) and CO (lower panel) mixing ratios from the MATCH-MPIC based chemical weather forecast and analysis system (solid lines). Observed mixing ratios are also plotted as asterisks (grey) with 3-h time intervals. The three events are marked by arrows (11–13, 17 and 24 September). Time axis is local time (UTC + 9 h). Also shown are scatter plots of observed versus modelled mixing ratios for O_3 and CO. The three events are given separate symbols.

intensive period. The CO in the model is separated into tagged contributions from fossil fuel and biomass burning sources in North America, South America, Western Europe, Eastern Europe, Northern Asia, Southern Asia, Africa and Australia, contributions from oxidation of methane and NMHC and from all remaining small sources such as ocean sources. In particular, North Asia is defined as two boxes (20°N–70°N, 60°E–150°E and 20°N–70°N, 90°E–150°E), which include the eastern part of Russia, China, Korea, Mongolia and Japan but exclude India, as described in Lawrence et al. (2003).

The model reproduces the general features for both O_3 and CO well, including baseline levels, and shows enhancements during each of the observed high mixing ratio episodes. For O_3, the observed variability is larger than modelled, likely due to physical factors on a local scale. The modelled O_3 day-to-day variations correspond more closely to the CO enhancements than in the observations. The model captures the enhanced mixing ratios on 17 and 24 September, peaking at 225 and 146 ppbv for CO, and 47 and 39 ppbv for O_3, respectively. The model exhibited slightly elevated peaks during 11–13 September, having the maximum mixing ratios of 219 (11 September) and 204 ppbv (13 September). However, the model underestimates the CO mixing ratios during this episode substantially, by up to 150 ppbv.

Scatter plots of the modelled versus observed mixing ratios for O_3 and CO during the intensive period are also displayed in Fig. 4. Excluding the 11–13 September period, the results show moderate correlations, with O_3 having a slightly lower correlation coefficient ($r = 0.41$) compared with CO ($r = 0.62$). The correlations between the modelled and observed O_3 and CO during the episodes on 17 and 24 September are similar to those during the remaining periods, suggesting that these events are well captured and reproduced by the model. In contrast, the data for the 11–13 September event shows the large discrepancy for CO between the model and the observations, as noted above.

We explore the contributions from primary sources to CO at Rishiri Island, as shown in Fig. 5. The simulated contribution from North Asia is about 75 ppbv on average and dominates the background level (note that the red line for the North Asian tracer is referenced to the left-hand axis, whereas the other tracers are referenced to the right-hand axis on the figure). The high-CO episodes on 11, 13, 17 and 24 September are clearly shaped by the North Asian sources. There are also two additional enhancements on 14 and 25 September in the model results, which are not observed (later in Fig. 6 it can be seen that the first is due to biomass burning and the second to fossil fuel burning emissions of CO). Other sources in the Northern Hemisphere (e.g. Europe and North America) only have about 10 ppbv contributions and are almost constant throughout the period. South Asia has a negligible contribution (i.e. 2 ppbv), as do the sources in the Southern Hemisphere. Relative contributions by source types indicate that major primary sources dominate the observed CO levels and account for more than 70% on average during the period. Secondary production from oxidation of methane and NMHC, as well as from other remaining small sources such as the ocean, only contributes 30%. North Asia is the dominant source, contributing about 50%, with the second largest contributing source being Europe (sum of Western and Eastern Europe, ~8%). North America is the third largest source (~7%). It should be noted that the North Asian source influences the 11–13 September episode to shape the small modelled peaks. However, the influence is too small to explain the observed CO mixing ratios. Given the relatively small general contributions of the other sources, it is unlikely that these can explain the discrepancy between the model and the observations for the 11–13 September event, thus clearly pointing toward a missing source in the North Asian region emissions inventory.

Contributions from primary sources in North Asia in the model are further deconvoluted into fossil fuel and biomass burning. Contributions from biomass burning are also examined

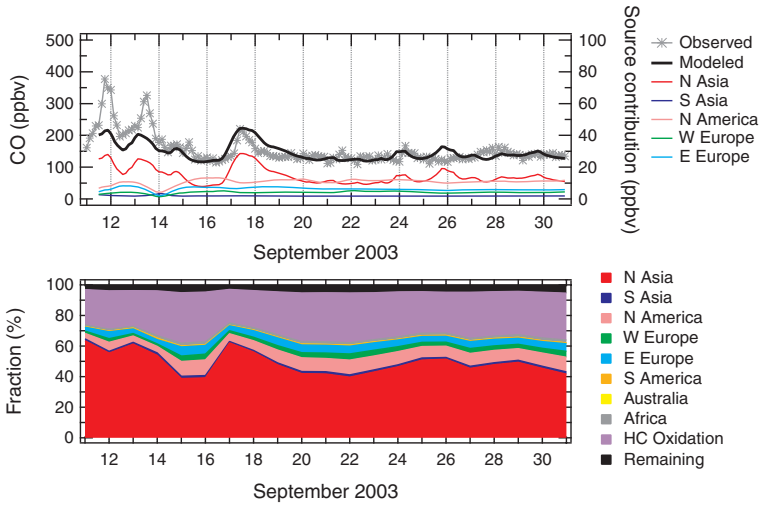

Fig. 5. Contributions from each emission source to CO simulated in the MATCH-MPIC model. Contributions from major source regions are shown in the absolute mixing ratios (upper panel) in which the red line for the North Asian tracer is referenced to the left-hand axis, whereas the other tracers are referenced to the right-hand axis; those from all sources are illustrated as relative fractions on a daily basis (lower). Time axis is local time (UTC + 9 h).

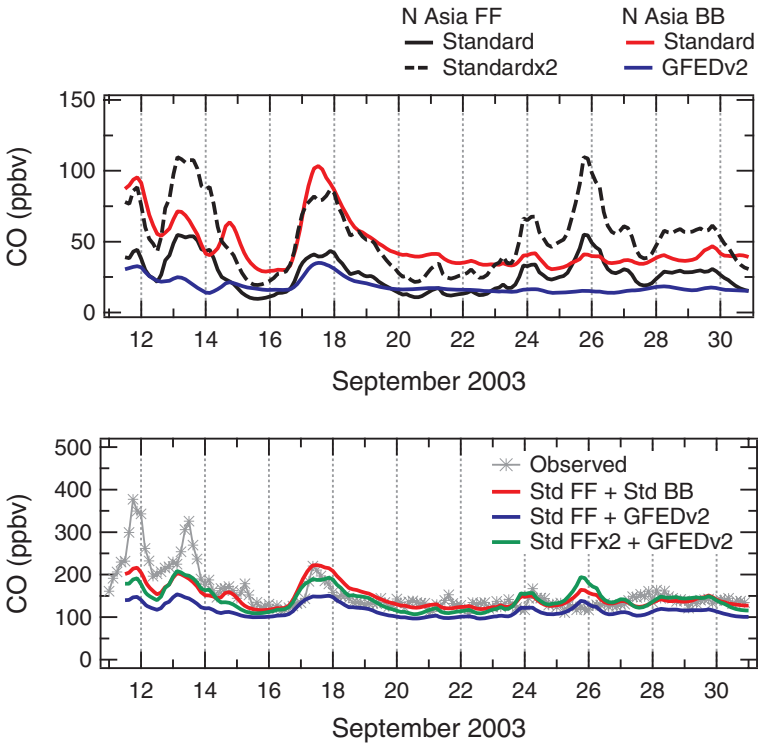

Fig. 6. Contributions from North Asian fossil fuel and biomass burning emission sources to CO simulated in the MATCH-MPIC model. Contributions from fossil fuel (FF) and biomass burning (BB) with two emissions inventories are shown (upper), and three time-series plots of the total CO simulated with the 'standard' emission and GFEDv2 are shown (lower). Time axis is local time (UTC + 9 h).

by comparing the results of simulations using the 'standard' and 'hybrid-GFEDv2' inventories, as shown in the upper graph of Fig. 6. Fossil fuel contributions are generally less than 50 ppbv. There are peaks corresponding to the three high-CO episodes, but they are all too small to fully explain the enhancements. For biomass burning, the 'standard' emissions from North Asia show larger contributions than fossil fuel for the baseline and the episodes on 11–13 and 17 September, though the two make comparable contributions to the peak on 24 September. Interestingly, the peaks in fossil fuel and biomass burning CO correspond roughly to each other. The degree of correlation of fossil fuel to biomass burning contributions in North Asia for the entire period are $r = 0.55$ ('standard' emissions) and 0.44 ('hybrid-GFEDv2' emissions), indicating a broad colocation of these emissions.

The simulation results with the 'hybrid-GFEDv2' inventory show much lower contributions from North Asian biomass burning, with the baseline being about a factor of two lower. The three episodes are still simulated, but also correspondingly weaker. Combined with GFEDv2, simulated total CO is about 30 ppbv lower than the observations. If we were to assume that the updated GFEDv2 emissions for 2003 are more accurate than the older climatological 'standard' emissions for the model, then this would imply that North Asian anthropogenic emissions would need to be increased in the model to reproduce the observations. Following on this hypothesis, we can examine what we would expect if the North Asian fossil fuel emissions were doubled, combined with the GFEDv2 biomass burning emissions, plotted as an additional line in Fig. 6. Note that this is not exactly what would result if the North Asian fossil fuel emissions were really doubled online in the model, due to the feedback via OH, but this provides a rough approximation. The figure shows that doubling fossil fuel emissions substantially enhances the CO baseline toward the observed levels and fills the gap between the observations and GFEDv2-based simulations, particularly for the latter two events. This is in reasonable accordance with the recent upward revision of Chinese CO emissions by Streets et al. (2006). Chinese CO emissions in their improved inventory are 157 Tg, and are approximately double those in EDGAR v3.2 (88 Tg). The Chinese CO emissions in the 'standard' inventory in the MATCH-MPIC model are 88 Tg, and hence doubling North Asian fossil fuel emissions is reasonable. More interesting is that the first event (11–13 September) is still greatly underestimated even if the contributions from North Asian fossil fuel emissions are increased.

3.4. *Tracking CO plumes by AIRS satellite measurements*

The Atmospheric Infrared Sounder (AIRS) was launched on the NASA Aqua satellite in May 2002. It is a cross-track scanning grating spectrometer covering the 3.7–16 μm spectral range with 2378 channels (Aumann et al., 2003). AIRS has a spatial resolution of 45 km at nadir and a 1650 km cross-track swath, providing daily global coverage of CO in the troposphere. Carbon monoxide retrievals are obtained at 4.7 μm, including for partly cloudy scenes (McMillan et al., 2005). Warner et al. (2007)

showed that AIRS has a positive bias of 15–20 ppbv over the oceans, relative to the Measurements of Pollution in the Troposphere (MOPITT) instrument onboard the EOS Terra satellite (Edwards et al., 1999). However, events of CO bursts can be clearly seen by AIRS (Yurganov et al., 2008). Hence we use AIRS observations (version 5) of CO total column to qualitatively illustrate daily maps of CO distributions and to track CO pollution plumes on a daily basis.

Neither of MOPITT and AIRS is sensitive to the boundary layer CO, although the maximum sensitivity by AIRS is slightly higher than MOPITT. The greater advantage of AIRS is its increased horizontal spatial coverage (70% of the globe each day, versus MOPITT, which takes about 3 d for the global coverage). This greater spatial coverage allows us to track CO plumes transported from the emission sources to distances of several thousands km on each day. It should be noted that the CO data at Rishiri Island are surface measurements at a single observatory, and the AIRS CO data are total column that is summed up from the surface to the upper atmosphere, with the maximum sensitivity to the middle troposphere. The ascending overpass of AIRS usually occurs during local daytime and the descending does during nighttime. We used swath data obtained during daytime (07:30–19:30 local time) to make a daily plot.

Figures 7–9 show daily distributions of CO total columns for three events during the intensive campaign in September 2003, illustrating intriguing roles of pollution plumes from industrial and wildfire sources. The CO total columns observed by AIRS are compared qualitatively with those modelled with 'hybrid-GFEDv2' and 'standard' emissions. A movie of the AIRS CO total columns during the whole campaign period can be seen separately (see Appendix S1 in Supporting Information).

For the 11–13 September event, the model underestimated the surface observations, suggesting the presence of additional influences. AIRS shows large and moderate CO enhancements over far eastern and western Siberia, respectively. The CO total column is higher over far eastern Siberia than western Siberia. The large CO enhancement over far eastern Siberia was being spread towards the south on 10 September. This plume moved eastwards (see B_1 and B_2), and did not directly impact northern Japan. Both simulations predicted this plume and successive transport, with the'hybrid-GFEDv2' based simulations indicating lower concentrations than the 'standard' based. The CO enhancements predicted with the 'hybrid-GFEDv2' emissions are not as widespread as those observed by AIRS or modelled with 'standard' emissions. Transport from eastern central China to the western Pacific was also detected. A high-CO belt stretching from China toward northern Japan was visible on 11 September (see C_1), and this feature was reproduced by the model simulations with both inventories. Interestingly, we are also able to see a CO plume originating from western Siberia toward northern Japan on 10 and 11 September, driven by eastward transport over Siberia (see A_1 and A_3). High CO episodes observed at the surface of Rishiri Island are likely due to this plume, which explains the discrepancy against the modelled enhancements. None of the simulations predicted this long-range transport of CO from western Siberia, whereas they exhibited some CO enhancements over burning locations of western Siberia. Since AIRS has almost no sensitivity to the boundary layer CO, the plumes detected by AIRS represent enhancements in the middle troposphere, which may or may not be associated with the boundary layer enhancements. However, Wild et al. (2004) reported that long-range transport of air across the Eurasian continent could differ significantly from that over the Pacific and Atlantic, and it mainly occurs in the boundary layer because of weaker and less frequent frontal systems over the Eurasian continent. The argument with respect to transport height of fire plumes is an important future issue to resolve.

AIRS shows substantial CO enhancement over far eastern Siberia. The AIRS also sees CO enhancement over western Siberia (A_5 and A_6). The simulations with 'hybrid-GFEDv2' emissions exhibit substantial and small CO enhancement over far eastern and western Siberia, respectively. According to the 8-d averaged GFEDv2 inventory, there are substantial and negligible fire activities over far eastern and western Siberia, respectively, during this period. The discrepancy between AIRS observations and model simulations could be because of underestimated CO emissions resulting from hotspots near the surface that are not clearly visible to thermal infrared (IR) satellites. The absence of profile smoothing by averaging kernels also could explain some differences. Pollution plumes from China are clearly seen during 16–18 September, showing a high-CO belt gradually spreading to the east (see C_2). Large CO plumes were first transported to the northeast, passed over northern Japan and then further moved over the western Pacific. This feature was simulated well by the model simulations.

The case for 24 September is much more obvious. The AIRS detected much smaller CO enhancement over far eastern Siberia, reflecting weakened fire activities at the end of September. Weakened burnings during this period allow us to track detailed features of pollution transport from China to northern Japan. Trajectories of CO plumes suggest that the air mass associated with high CO levels over eastern central China gradually moved towards the northeast, passed over northern Japan and then further transported to the western Pacific in a time scale of days (see C_3). The model simulations with both inventories successfully reproduced this regional-scale transport of CO. The CO enhancements in the 'hybrid-GFEDv2' simulation were lower than in the 'standard' emissions simulation due to absence of co-located biomass burning emissions in East Asia. Also interesting is that high-CO bands are visible over western Siberia in spite of very small burning activities during this period. The plume was transported eastwards in a long distance over days (A_6 and A_7). Since both simulations well reproduced this plume, this is likely trans-Eurasian transport of CO emitted from Europe, not from wildfires.

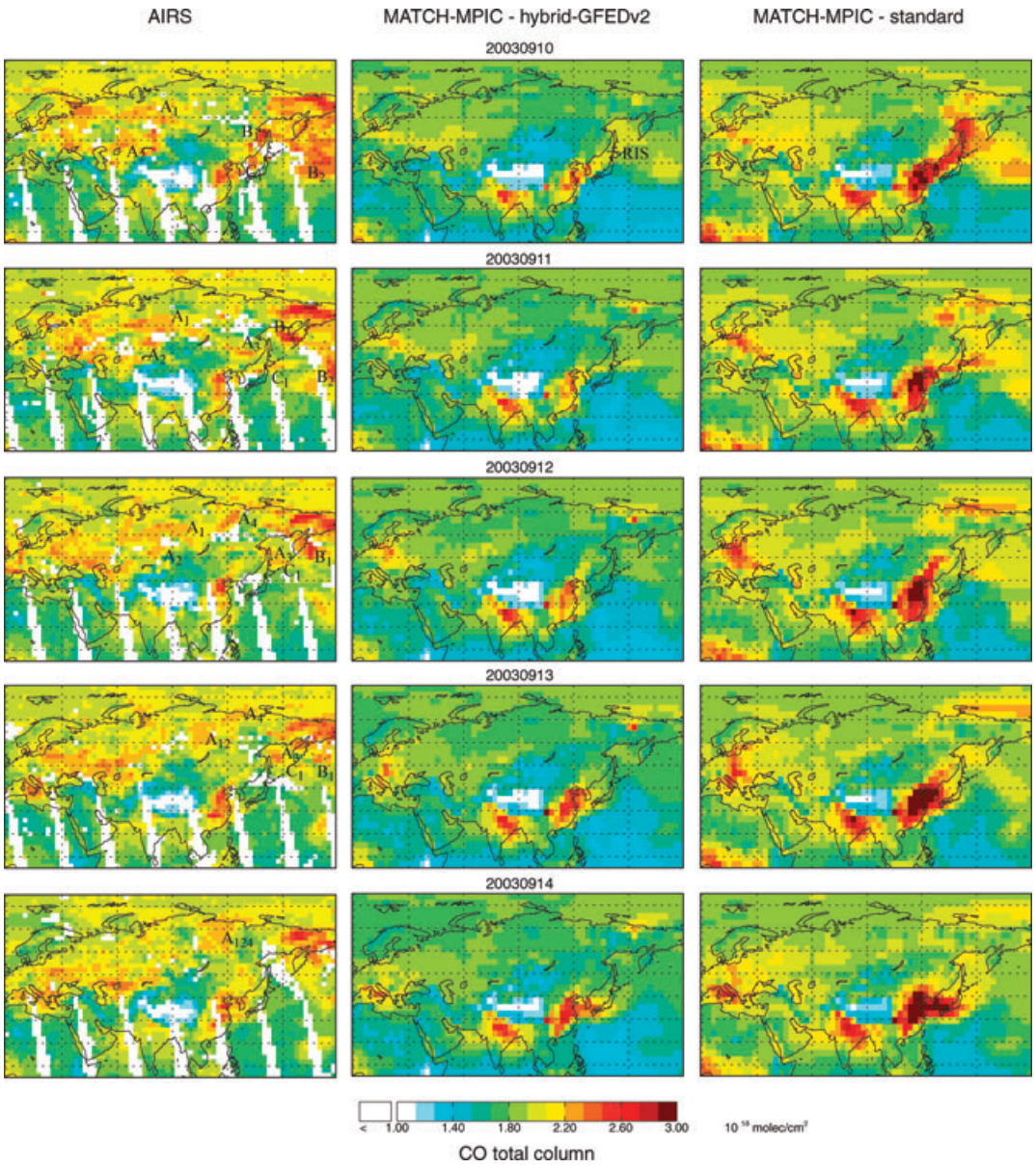

Fig. 7. Daily distributions of CO total columns derived from the AIRS satellite observations (left-hand column) and from the MATCH-MPIC model simulations based on 'hybrid-GFEDv2' (middle column) and 'standard' (right column) emissions inventories from 10 to 14 September 2003. A, B, and C denote high-CO air masses originated from western Siberia, far eastern Siberia and eastern central China, respectively. Location of Rishiri Island (RIS) is noted.

To summarize, the model with 'hybrid-GFEDv2' emissions predicted CO enhancement over burning regions in western and far eastern Siberia throughout the three events. This feature is qualitatively good agreement with AIRS observations. However, the CO enhancements in 'hybrid-GFEDv2'-based simulations were much smaller and less widespread than those observed by AIRS and modelled with 'standard emissions'. This could be because CO emissions per area were underestimated in the GFEDv2 inventory. Another reason could be that the GFEDv2 inventory failed to implement small fires since not all fires are clearly visible from space, although satellite-derived hot spots generally correspond to actual fires.

Since the burning area in western Siberia is known to contain large amounts of peat and buried carbon, main burning in western Siberia could be peat burning. The emission estimates for western Siberia could be smaller than actual due to undercounting hotspots by satellite measurements, especially in case of smouldering. Peat burning is mainly smouldering. The underestimate in CO emissions may thus be associated with estimates of peat burning. The total emission of CO (and other trace gases and

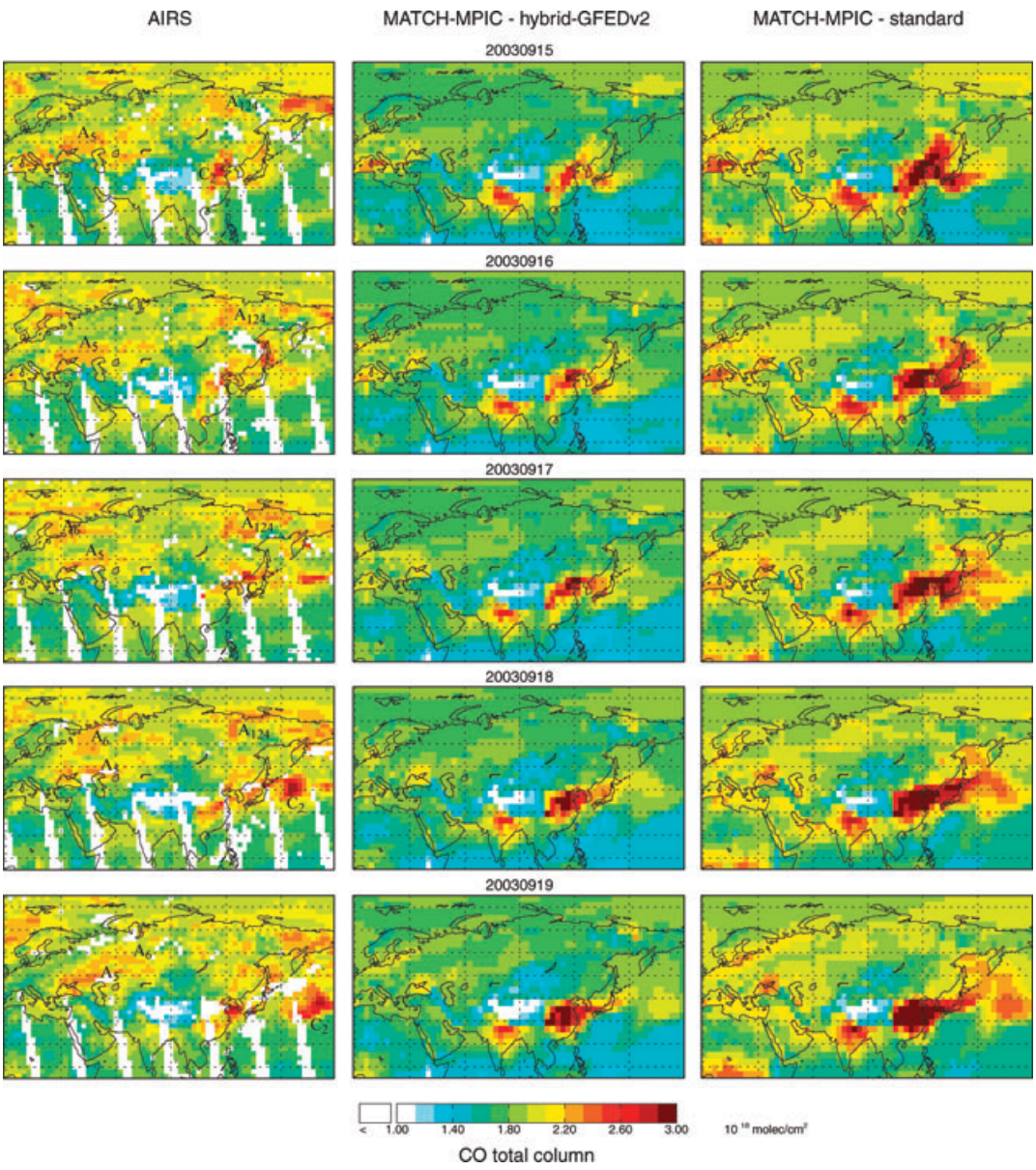

Fig. 8. Same as Figure 7 but from 15 to 19 September 2003.

aerosols) from peat burning seems extremely difficult to assess, due to large uncertainties such as the amount of organic matter, depth of organic layers and soil moisture under the ground surface. The emission factors of trace gases from peat burnings may be greatly different from the Andreae and Merlet (2001) 'standard' values, which are commonly used in current emissions inventories. All of these factors enhance the uncertainty in estimating CO emissions. Although the GFEDv2 inventory is one of the state-of-science inventories for biomass burning emissions, the detailed analyses of day-to-day CO variations with a modern satellite sensor implies that it may still need improvements for boreal fires in Siberia.

4. Conclusions

Following the extensive fire season of summer 2003, an intensive field campaign was performed on the island of Rishiri, a remote small island in northern Japan. During an intensive campaign, three enhanced CO episodes were identified. Although the O_3 versus CO relationship during two episodes (17 and 24 September) was in the typical range observed in September of other years, the relationship during the other episode (11–13 September) showed significant biases towards CO, being indicative of biomass burning influences from Siberia. However, the BC to CO relationship during 11–13 September showed lower BC/CO

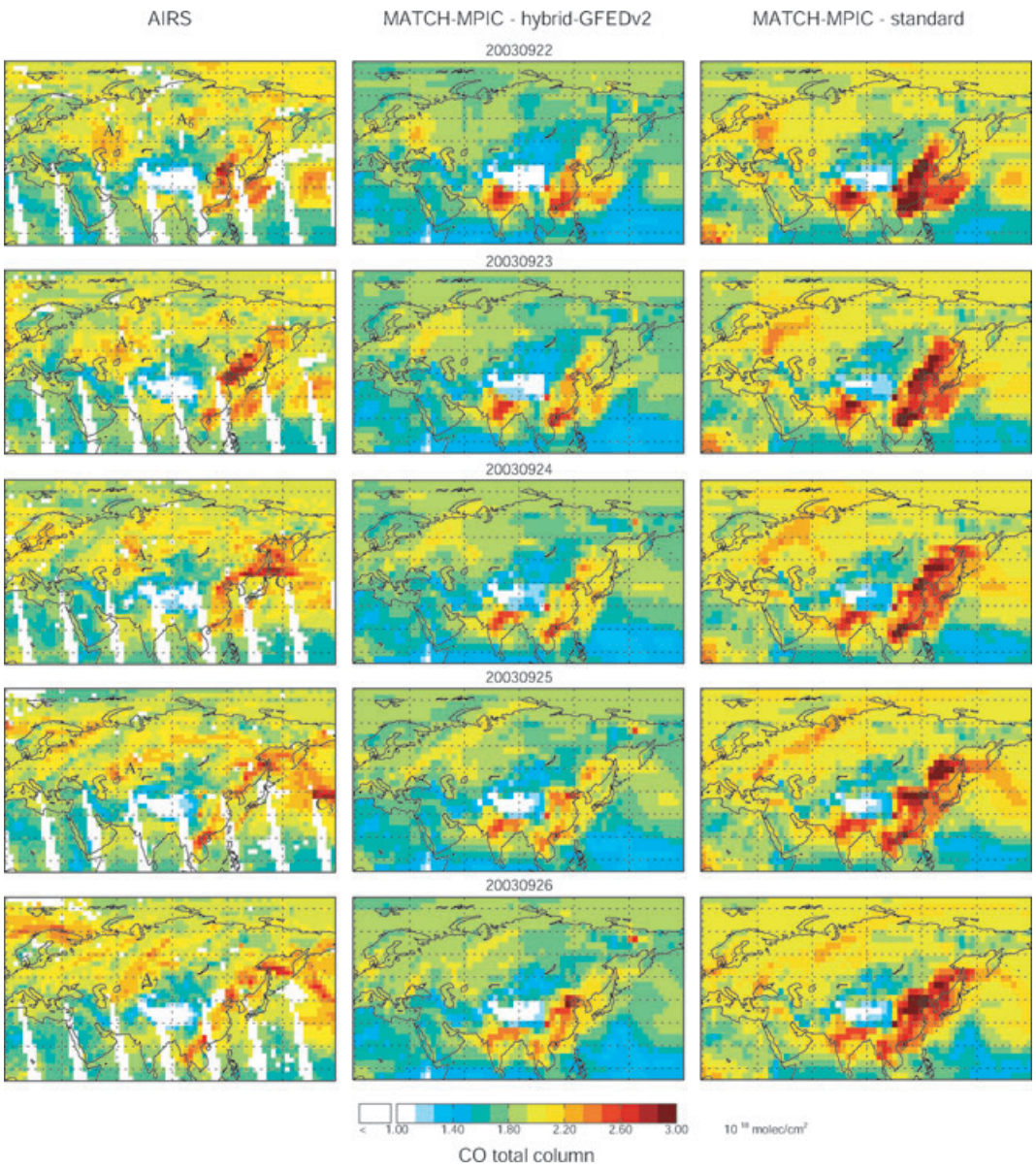

Fig. 9. Same as Figure 7 but from 22 to 26 September 2003.

ratios than in the other two episodes, probably as a result from efficient removal of BC during long-range transport, making the interpretation of this episode ambiguous.

The MATCH-MPIC chemical weather forecast and analysis system captured the general features for basic chemical tracers, O_3 and CO, and indicated that the CO budget at Rishiri Island was mainly dominated by North Asian sources, which contributed about 50% on average, and as much as nearly 60% during enhancement episodes. The model captured the timing and magnitude of the enhancements in CO in two pollution episodes around 17 and 24 September. The model, however, substantially underestimated the magnitude of the CO enhancement for an event during 11–13 September. For North Asian emissions, contributions from fossil fuel and biomass burning sources were separated. Two emissions inventories were compared for biomass burning sources for CO. The 'standard' climatological biomass burning emissions implemented in the MATCH-MPIC model produced substantially higher CO at Rishiri Island than 'hybrid-GFEDv2' emissions, which is based on a satellite-derived emissions inventory, and hence is expected to be more accurate and realistic for 2003 than the climatological inventory. On the contrary, industrial emissions from China in the MATCH-MPIC 'standard' inventory were found to be 45% lower than recent estimates by Streets et al. (2006). The overestimates in biomass burning sources compensated for the underestimates in fossil fuel sources in the 'standard' inventory. Coupled with biomass

burning emissions from GFEDv2, doubled contributions from fossil fuel emissions in the 'standard' inventory provided reasonable agreement for general baseline levels and variability, including the magnitude for the events on 17 and 24 September. However, this still underestimated the amplitude for the 11–13 September episode, further suggesting the presence of a missing or underestimated CO source in this region.

Satellite images from AIRS were examined to identify possible CO enhancements and to track pollution plumes on a daily basis. AIRS revealed visible enhancement of CO from wildfires over western and far eastern Siberia, and from human activities over eastern central China. AIRS clearly captured regional-scale transport of CO from Chinese sources to the western Pacific. The location of CO enhancements detected by AIRS in far eastern and western Siberia was in general accordance with those by the GFEDv2-based simulations. However, AIRS-derived CO enhancements are larger and more widespread than modelled with GFEDv2 over Siberia. These results indicate that CO emissions from wildfires, especially in western Siberia, are likely underestimated in the state-of-science emissions inventories due to a number of uncertainties in building emissions inventory for biomass burning.

5. Acknowledgments

We acknowledge Mitsuo Uematsu (University of Tokyo) and Miori Ohno (National Institute for Environmental Studies) for providing technical help. We are grateful to Leonid N. Yurganov (University of Maryland) for valuable comments and suggestions on the initial manuscript. We thank Daniel J. Jacob (Harvard University) for hosting H.T. and the use of Atmospheric Chemistry Modeling Group resources. This work was supported by Asian Environment Research Program at National Institute for Environmental Studies. AIRS data are obtained at the NASA's Atmospheric Composition Data and Information Services Center (ACDISC).

References

Andreae, M. O. and Merlet, P. 2001. Emission of trace gases and aerosols from biomass burning. *Global Biogeochem. Cycles* **15**, 955–966.

Aumann, H. H., Chahine, M. T., Gautier, C., Goldberg, M. D., Kalnay, E. and co-authors. 2003. AIRS/AMSU/HSB on the Aqua mission: sesign, science objectives, data products and processing systems. *IEEE Trans. Geosci. Remote Sens.* **41**, 253–264.

Dickerson, R. R., Andreae, M. O., Campos, T., Mayol-Bracero, O. L., Neususess, C. and co-authors. 2002. Analysis of black carbon and carbon monoxide observed over the Indian Ocean: implications for emissions and photochemistry. *J. Geophys. Res.* **107**, 8017, doi:10.1029/2001JD000501.

Edwards, D. P., Halvorson, C. M. and Gille, J. C. 1999. Radiative transfer modeling for the EOS Terra satellite measurement of pollution in the troposphere (MOPITT) instrument. *J. Geophys. Res.* **104**, 16 755–16 775.

Galanter, M., Levy, H. and Carmichael, G. R. 2000. Impacts of biomass burning on tropospheric CO, NOx, and O_3. *J. Geophys. Res.* **105**, 6633–6653.

Jaffe, D., Bertschi, I., Jaeglé, L., Novelli, P., Reid, J. S. and co-authors. 2004. Long-range transport of Siberian biomass burning emissions and impact on surface ozone in western North America. *Geophys. Res. Lett.* **31**, L16106, doi:10.1029/2004GL020093.

Kanaya, Y., Cao, R., Kato, S., Miyakawa, Y., Kajii, Y. and co-authors. 2007. Chemistry of OH and HO_2 radicals at Rishiri Island, Japan, in September 2003: missing sink of HO_2 in the daytime and positive correlations with monoterpenes in the nighttime. *J. Geophys. Res.* **112**, D11308, doi:10.1029/2006jd007987.

Kaneyasu, N. and Murayama, S. 2000. High concentrations of black carbon over middle latitudes in the North Pacific Ocean. *J. Geophys. Res.* **105**, 19 881–19 890.

Kaneyasu, N. and Takada, H. 2004. Seasonal variations of sulfate, carbonaceous species (black carbon and polycyclic aromatic hydrocarbons), and trace elements in fine atmospheric aerosols collected at subtropical islands in the East China Sea. *J. Geophys. Res.* **109**, D06211, doi:10.1029/2003JD004137.

Kaneyasu, N., Igarashi, Y., Sawa, Y., Takahashi, H., Takada, H. and co-authors. 2007. Chemical and optical properties of 2003 Siberian forest fire smoke observed at the summit of Mt. Fuji, Japan. *J. Geophys. Res.* **112**, D13214, doi:10.1029/2007JD008544.

Kato, S., Miyakawa, Y., Kaneko, T. and Kajii, Y. 2004. Urban air measurements using PTR/MS in Tokyo area and comparison with GC-FID measurements. *Int. J. Mass Spectrom.* **235**, 103–110.

von Kuhlmann, R., Lawrence, M. G., Crutzen, P. J. and Rasch, P. J. 2003. A model for studies of tropospheric ozone and nonmethane hydrocarbons: model description and ozone results. *J. Geophys. Res.* **108**, 4294, doi:10.1029/2002JD002893.

Lawrence, M. G., Crutzen, P. J., Rasch, P. J., Eaton, B. E. and Mahowald, N. M. 1999. A model for studies of tropospheric photochemistry: description, global distributions, and evaluation. *J. Geophys. Res.* **104**, 26 245–26 277.

Lawrence, M. G., Rasch, P. J., von Kuhlmann, R., Williams, J., Fischer, H. and co-authors. 2003. Global chemical weather forecasts for field campaign planning: predictions and observations of large-scale features during MINOS, CONTRACE, and INDOEX. *Atmos. Chem. Phys.* **3**, 267–289.

Matsumoto, K., Uematsu, M., Hayano, T., Yoshioka, K., Tanimoto, H. and co-authors. 2003a. Simultaneous measurements of particulate elemental carbon on the ground observation network over the western North Pacific during the ACE-Asia campaign. *J. Geophys. Res.* **108**, 8635, doi:10.1029/2002JD002744.

Matsumoto, K., Uyama, Y., Hayano, T., Tanimoto, H., Uno, I. and co-authors. 2003b. Chemical properties and outflow patterns of anthropogenic and dust particles on Rishiri Island during the Asian Pacific Regional Aerosol Characterization Experiment (ACE-Asia). *J. Geophys. Res.* **108**, 8666, doi:10.1029/2003JD003426.

McMillan, W. W., Barnet, C., Strow, L., Chahine, M., Warner, J. and co-authors. 2005. Daily global maps of carbon monoxide from NASA's Atmospheric Infrared Sounder. *Geophys. Res. Lett.*, **32**, L11801, doi:10.1029/2004GL021821.

Novakov, T., Andreae, M. O., Gabriel, R., Kirchstetter, T. W., Mayol-Bracero, O. L. and co-authors. 2000. Origin of carbonaceous aerosols over the tropical Indian Ocean: biomass burning or fossil fuels? *Geophys. Res. Lett.* **27**, 4061–4064.

Okuda, T., Tenmoku, M., Kato, J., Mori, J., Sato, T. and co-authors. 2006. Long-term observation of trace metal concentration in aerosols at a remote island, Rishiri, Japan by using inductively coupled plasma mass spectrometry equipped with laser ablation. *Water Air Soil Pollut.* **174**, 3–17.

Olivier, J. G. J. and Berdowski, J. J. M. 2001. Global emissions sources and sinks. In: *The Climate System* (eds J. Berdowski, R. Guicherit, and B.J. Heij). A. A. Balkema Publishers/Swets & Zeitlinger Publishers, Lisse, The Netherlands, 33–78, ISBN 90 5809 255 0.

Olivier, J. G. J., Berdowski, J. J. M., Peters, J. A. H. W., Bakker, J., Visschedijk, A. J. H. and co-authors. 2002. Applications of EDGAR. Including a description of EDGAR 3.2: reference database with trend data for 1970–1995. *RIVM report 773301 001/NRP report 410 200 051*, RIVM,Bilthoven.

Parrish, D. D., Holloway, J. S., Trainer, M., Murphy, P. C., Forbes, G. L. and co-authors. 1993. Export of North American ozone pollution to the North Atlantic Ocean. *Science,* **259**, 1436–1439.

Parrish, D. D., Trainer, M., Holloway, J. S., Yee, J. E., Warshawsky, M. S. and co-authors. 1998. Relationships between ozone and carbon monoxide at surface sites in the North Atlantic region. *J. Geophys. Res.*, **103**, 13 357–13 376.

Rasch, P. J., Mahowald, N. M. and Eaton, B. E. 1997. Representations of transport, convection and the hydrologic cycle in chemical transport models: implications for the modeling of short lived and soluble species. *J. Geophys. Res.* **102**, 28 127–28 138.

Streets, D. G., Zhang, Q., Wang, L., He, K., Hao, J. and co-authors. 2006. Revisiting China's CO emissions after the Transport and Chemical Evolution over the Pacific (TRACE-P) mission: synthesis of inventories, atmospheric modeling, and observations. *J. Geophys. Res.* **111**, D14306, doi:10.1029/2006JD007118.

Tanimoto, H., Kajii, Y., Hirokawa, J., Akimoto, H. and Minko, N. P. 2000. The atmospheric impact of boreal forest fires in far eastern Siberia on the seasonal variation of carbon monoxide: observations at Rishiri, a northern remote island in Japan. *Geophys. Res. Lett.* **27**, 4073–4076.

Tanimoto, H., Furutani, H., Kato, S., Matsumoto, J., Makide, Y. and co-authors. 2002. Seasonal cycles of ozone and oxidized nitrogen species in Northeast Asia, 1: impact of regional climatology and photochemistry observed during RISOTTO 1999–2000. *J. Geophys. Res.* **107**, 4747, doi:10.1029/2001JD001496.

Tanimoto, H., Sawa, Y., Yonemura, S., Yumimoto, K., Matsueda, H. and co-authors. 2008a. Diagnosing recent CO emissions and ozone evolution in East Asia using coordinated surface observations, adjoint inverse modeling, and MOPITT satellite data. *Atmos. Chem. Phys.* **8**, 3867–3880.

Tanimoto, H., Matsumoto, K. and Uematsu, M. 2008b. Ozone–CO correlations in Siberian wildfire plumes observed at Rishiri Island. *SOLA* **4**, 65–68.

Warner, J., Comer, M. M., Barnet, C. D., McMillan, W. W., Wolf, W. and co-authors. 2007. A comparison of satellite tropospheric carbon monoxide measurements from AIRS and MOPITT during INTEX-A. *J. Geophys. Res.* **112**, D12S17, doi:10.1029/2006JD007925.

van der Werf, G. R., Randerson, J. T., Giglio, L., Collatz, G. J., Kasibhatla, P. S. and co-authors. 2006. Interannual variability in global biomass burning emissions from 1997 to 2004. *Atmos. Chem. Phys.* **6**, 3423–3441.

Wild, O., Pochanart, P. and Akimoto, H. 2004. Trans-Eurasian transport of ozone and its precursors. *J. Geophys. Res.* **109**, D11302, doi:10.1029/2003JD004501.

Yurganov, L. N., Blumenstock, T., Grechko, E. I., Hase, F., Hyer, E. J. and co-authors. 2004. A quantitative assessment of the 1998 carbon monoxide emission anomaly in the Northern Hemisphere based on total column and surface concentration measurements. *J. Geophys. Res.* **109**, D15305, doi:10.1029/2004JD004559.

Yurganov, L. N., Duchatelet, P., Dzhola, A. V., Edwards, D. P., Hase, F. and co-authors. 2005. Increased Northern Hemispheric carbon monoxide burden in the troposphere in 2002 and 2003 detected from the ground and from space. *Atmos. Chem. Phys.* **5**, 563–573.

Yurganov, L. N., McMillan, W. W., Dzhola, A. V., Grechko, E. I., Jones, N. B. and co-authors. 2008. Global AIRS and MOPITT CO measurements: validation, comparison, and links to biomass burning variations and carbon cycle. *J. Geophys. Res.* **113**, D09301, doi:10.1029/2007JD009229.

Supporting Information

Additional Supporting Information may be found in the online version of this article.

Appendix S1. GIF animation of AIRS CO total column in September 2003.

Please note: Wiley-Blackwell are not responsible for the content or functionality of any supporting materials supplied by the authors. Any queries (other than missing material) should be directed to the corresponding author for the article.